Environ. Sci. Technol. 1998, 32, 1092−1098

# Selenium Diffusion and Reduction at the Water−Sediment Boundary: Micro-XANES Spectroscopy of Reactive Transport

TETSU K. TOKUNAGA*
*Earth Sciences Division, E. O. Lawrence Berkeley National Laboratory, 1 Cyclotron Road, 90-1116, Berkeley, California 94720*

STEPHEN R. SUTTON
*Department of Geophysical Sciences and Consortium for Advanced Radiation Sources, The University of Chicago, 5640 South Ellis Avenue, Chicago, Illinois 60637*

SASA BAJT
*Lawrence Livermore National Laboratory, P.O. Box 808, L-395, Livermore, California 94550*

PATTERSON NUESSLE
*Advanced Analytical Center for the Environmental Sciences, Savannah River Ecology Laboratory, University of Georgia, P.O. Drawer E, Aiken, South Carolina 29802*

GRACE SHEA-MCCARTHY
*Brookhaven National Laboratory, Building 901A, Upton, New York 11973*

Mechanistic understanding of trace element cycling between surface waters and sediments can require highly spatially resolved information at water−sediment boundaries not obtainable by conventional sampling and analytical methods. This study demonstrates the application of micro-X-ray absorption near-edge structure (micro-XANES) spectroscopy for obtaining such direct, in-situ, spatially and temporally resolved information for selenium. The experiments determine the fate of soluble Se(VI) ponded over water-saturated oxidizing versus reducing sediments. Scanning micro-XANES analyses showed Se(VI) removal from ponded waters by diffusion into sediments and by conversion to Se(0) in the reducing sediment. Zones of accumulation of insoluble Se(0) were heterogeneously distributed. These results show that the scale over which volume averaging of chemical species is performed at sediment−water boundaries must be selected carefully and that the spatial resolution offered by micro-XANES is well-suited for these types of investigations.

## Introduction

An important step in the cycling of many trace elements in the environment involves transport across boundaries between surface waters and underlying sediments. This macroscopic interface between two environmental compartments is often chemically and biologically stratified because of steep gradients in dissolved oxygen and other major redox-controlling species (*1*−*3*). Anoxic conditions that often occur at very shallow sediment depths promote reduction of redox-sensitive trace elements that move into this boundary region. For many elements dissolved in natural and contaminated waters, redox transformation results in adsorption or precipitation, often at depths of only a few millimeters from the sediment surface. Selenium is an environmentally important trace element, both as an essential nutrient and a potential toxin, that undergoes such redox transformations (*4*−*6*). The often microbially mediated reduction from the water-soluble Se(VI) to adsorbable Se(IV) and further reduced forms [organo-Se, Se(0), Se(−II)] accounts for accumulation of this element in wetland sediments (*7*−*10*). Recently, it has been shown that abiotic Se reduction can also take place in the presence of Fe(II) common in anoxic environments (*11*). Selenium transport and transformations in wetlands has received considerable attention since the identification of Se poisoning in wildlife deaths and deformities at Kesterson Reservoir, California (*12, 13*). Wide variations in Se solubility and sorption characteristics among its different forms require that its speciation be understood in order to predict transport between compartments. Knowledge of the influence of other chemical species on Se transformations is important, as shown in previous studies which demonstrated that nitrate inhibits Se(VI) reduction in soils and contaminated agricultural drainwaters (*14*−*17*).

To test models of time-dependent trace element partitioning in surface water−sediment environments, experimental methods with appropriate spatial and temporal resolution are required. Determination of concentration profiles with adequate spatial resolution is critical since this is the basis upon which mass transfer calculations are performed. Sampling of sediments or pore waters required for various conventional laboratory analytical methods locally perturbs the system under investigation. Furthermore, speciation of sampled sediments based on sequential extraction methods may yield ambiguous results (*18*−*20*). Microelectrodes allow in-situ monitoring of $O_2$, pH, and a number of other chemical species but do not permit quantitative measurement of many elements and can require careful attention to interferences (*21*). Electron microprobe techniques offer superior spatial resolution but require sample exposure to a vacuum environment and to extreme local energy deposition rates. Limitations of all of the above approaches are most severe when investigating time-dependent processes, since it is then desirable to periodically determine spatial distributions of various chemical species. To our knowledge, measurements of Se at the water−sediment boundary have not previously been accomplished with the spatial resolution necessary to simultaneously quantify transport and reduction reactions. Such highly spatially and temporally resolved measurements are required to identify mechanisms controlling Se partitioning between surface waters and sediments.

The synchrotron X-ray fluorescence microprobe (SXRFM) permits nondestructive, two-dimensional mapping of a wide variety of trace elements under realistic environmental conditions, i.e., at atmospheric pressure and in the presence of relevant fluid phase(s). When applied to thin-sectioned samples, the SXRFM provides spatial resolution approaching 1 $\mu$m (*22, 23*). When the major reactions of concern involve oxidation−reduction of an element, the synchrotron-based technique of X-ray absorption near-edge structure (XANES) spectroscopy permits direct determination of formal valence

* Corresponding author e-mail: tktokunaga@lbl.gov; phone: (510) 486-7176; fax: (510) 486-5686.



S0013-936X(97)00655-X CCC: $15.00 
Published on Web 03/10/1998

(*24–27*). With increased oxidation state, core level electrons probed in K-edge XANES spectroscopy are less shielded and have increased transition probabilities to valence levels. These factors give rise to shifts in the main absorption edge to higher energies (typically a few eV per oxidation state) and to increased intensity of the first edge peak with increased valence. The valence sensitivity of XANES spectroscopy has been demonstrated in oxidation state studies of various elements (e.g., refs *28–30*).

Recently, XANES has been used to determine Se oxidation states in contaminated soils from Kesterson Reservoir and to track Se reduction in sediments during flooding (*31, 32*). Those studies demonstrated that the K-edge XANES of Se are useful in identifying its distribution among possible oxidation states in environmental systems. Mass transfer analyses and SXRFM data from that previous study indicated that Se reduction reactions were largely confined to very shallow depths within sediment columns (*33*). Mass transfer lengths of 6 and 35 mm were obtained for Se in these sediments, with most of the Se reduction taking place within these shallow depths. The previous study examined the case where seleniferous waters were ponded over initially partially water-saturated (42%) sediments such that some advection and initially high oxygen concentrations both promoted Se(VI) transport. Introduction of Se(VI) into ponded waters overlying already water-saturated sediments could result in even shorter mass transfer distances because of likely preexisting reducing conditions. These considerations pointed to the need for real time, in-situ, spatially resolved studies focused at the water–sediment boundary under established reducing conditions in order to improve our understanding of reactive Se transport under conditions common in ponded environments.

By combining monochromatic synchrotron radiation with the SXRFM, scanning micro-XANES spectroscopy (*34–36*) can be performed within very small regions (currently about 10 $\mu$m for trace elements). By scanning a sample in front of a monochromatic microbeam, micro-XANES can be used to obtain maps of spatial distributions of trace elements, including information on distributions among oxidation state (*37*). The study presented here utilized micro-XANES to obtain spatially and temporally resolved information needed to better understand diffusion and redox influences on Se transport across the water–sediment boundary. Experiments were conducted in small, ponded sediment columns with and without a large excess of $NO_3^-$ in order to inhibit and permit Se reduction, respectively.

## Materials and Methods

Small soil columns were designed to permit real time, in-situ SXRFM and micro-XANES measurements of vertical profiles of Se concentrations across ponded water–sediment boundaries. For each of two columns, rectangular 31 mm by 10 mm by 5 mm (height, width, and depth, respectively) cavities were milled into the middle of a 50 mm by 50 mm by 13 mm thick acrylic plastic sheet (Figure 1). A vertical hole (2.5 mm diameter) was drilled into the central cavity from the top edge to permit hypodermic syringe needle injection (and removal) of aqueous solutions, venting to atmospheric pressure, and periodic insertion of a calomel reference microelectrode. The backside of each cell was embedded with an array of platinum electrodes (spaced at 2–5 mm depth intervals) for redox potential measurements. The soil (Turlock sandy loam, Albic Natraqualf, surface 0.15 m soil) used for these columns was the same used in previous studies (*31–33*) collected from Kesterson National Wildlife Refuge in an area with no previous history of exposure to seleniferous waters. Only the <52 $\mu$m particle-size fraction of the soil was used in order to decrease grain-size associated

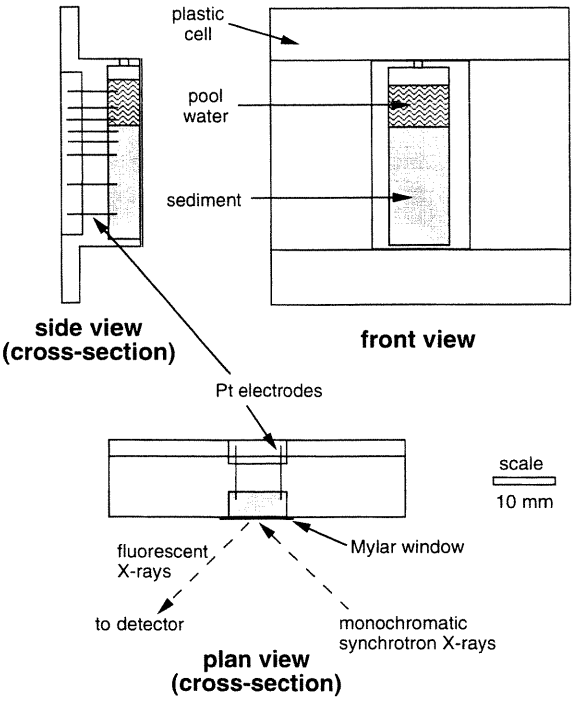


**FIGURE 1. Experimental cell design.**

**TABLE 1. Differences between Ponded Sediment Columns +N and −N[a]**

| column | | +N | −N |
|---|---|---|---|
| added organic matter | | 0 | 1% |
| preconditioning solution, mM | Na | 240 | 240 |
| | $SO_4$ | 0 | 120 |
| | $NO_3$ | 240 | 0 |
| replacement pool water | Na | 240 | 240 |
| | $SO_4$ | 0 | 115 |
| | $NO_3$ | 230 | 0 |
| | $SeO_4$ | 4.8 | 4.8 |

[a] See refs 31–33 for additional information on sediment properties.

variability in X-ray microbeam fluorescence. The organic matter content and total Se concentrations in the soil were 3% and <1 mg $kg^{-1}$, respectively. Soil was initially saturated with the two different solutions listed in Table 1. In the first ponded sediment system, denoted as +N, soil was saturated with a 240 mM $NaNO_3$ solution in order to maintain oxidizing conditions. In the second system, denoted as −N, organic matter in the form of air-dried and pulverized (<52 $\mu$m) grass (*Bromus mollis*) tissue was added uniformly into the soil to promote development of reducing conditions. The −N sediment was saturated with a 120 mM $Na_2SO_4$ solution. The appropriate preconditioning solution was added to the air-dry soil, mixed, compressed into a pellet, and compacted into the lower 20 mm portion of the acrylic frame. The bulk density, porosity, and saturation of the pellet were 1.28 Mg $m^{-3}$, 0.52, and 0.98, respectively. Adhesive Mylar tape was used to seal the front surface of each cell. Upon sealing, each column was oriented vertically and ponded with the same solution used to presaturate its sediment. The columns were maintained in vertical orientation and incubated in a room temperature water reservoir. The water reservoir served to minimize artifacts from oxygen diffusion across the Mylar windows and into sediments. The +N and −N columns were incubated for 2 and 5 days, respectively, prior to introduction of Se. The +N column was incubated for a shorter time to minimize the extent of $NO_3$ reduction, which would com-

promise the intended poising of redox potentials at high levels. Following this incubation period, the ponded solution was removed from each column with a syringe and immediately replaced with a solution containing Se(VI). This solution contained $SeO_4^{2-}$ at a concentration of 4.8 mM (380 mg of Se $L^{-1}$), with the background electrolyte composition similar to that of the preconditioning solutions (Table 1). The sediment columns were then monitored using the SXRFM in monochromatic mode, as described later. Between microprobe scans, the columns were kept in the room temperature water reservoir.

Redox potentials were measured periodically within each cell during the preconditioning interval and the micro-XANES experiment. For these measurements, the reference terminal of a millivolt meter was connected to a miniature calomel electrode that was dipped into the pool surface from the top access hole. The measuring terminal was sequentially connected to each of the Pt electrodes within the cell to obtain redox potential readings. The pH of pool waters was measured only upon removal from sample cells, at the time of removal of nonseleniferous pool water withdrawal, and at the end of the experiment.

Upon introduction of Se, each ponded sediment column was periodically scanned to obtained spatial distributions of total Se concentrations. Within selected locations, the partitioning of Se among possible oxidation states was determined through micro-XANES. Micro-XANES measurements were made on beamline X26A at the National Synchrotron Light Source (Brookhaven National Laboratory, NY). Details of this beamline and its components are provided elsewhere (*23, 34–37*). In brief, X-rays from the X26 bending magnet pass through a beamline aperture, Si channel-cut monochromator, ellipsoidal focusing mirror, slits, and ion chamber before interacting with the sample. The smallest incremental energy change achieved with the monochromator stepper motor is 0.35 eV at the Se(0) K-edge (12.658 keV), which is small as compared to the natural line width of about 2.3 eV (*38*). The ellipsoidal focusing mirror has a high energy cutoff of about 14 keV and therefore also serves to reject higher energy harmonics from the monochromator. A large spot size of about 200 $\mu$m was used in order to maintain high X-ray fluxes and average over many grains. In addition to this areal averaging along the front sample surface exposed to the incident beam, the detected signal includes depth-distributed fluorescence. The $e^{-1}$ X-ray penetration depth at the Se K-edge in the sediment is about 250 $\mu$m. Se, Fe, and Zn were detected in fluorescence mode with an energy dispersive Si(Li) detector. An 85 $\mu$m thick Al foil was placed over the detector face to suppress fluorescent radiation from major matrix elements (primarily from Fe), thereby decreasing detector dead times. Ponded sediment columns were scanned vertically in front of the beam using a motorized stage to obtain profiles of total Fe, Zn, and Se. The normalized Fe and Zn fluorescence permitted independent identification of the location of the pool–sediment boundary. Other matrix elements yielded weaker fluorescence in response to incident X-rays in the Se K-edge energy range and were not used for boundary location. Columns were moved in 0.50 mm vertical increments with each position in the beam path for 10 s (live counting time, dead time <30%). Total Se scans were performed with the monochromator set to 12.78 keV, well above the main absorption edges of Se such that species-specific differences in X-ray absorption are small. Concentrations were determined using water and sediment standards having known amounts of Se. Individual vertical profile scans typically required about 10 min. About 10 depth profile scans were obtained on each column with intervening times between profiling used to obtain XANES of standard samples and

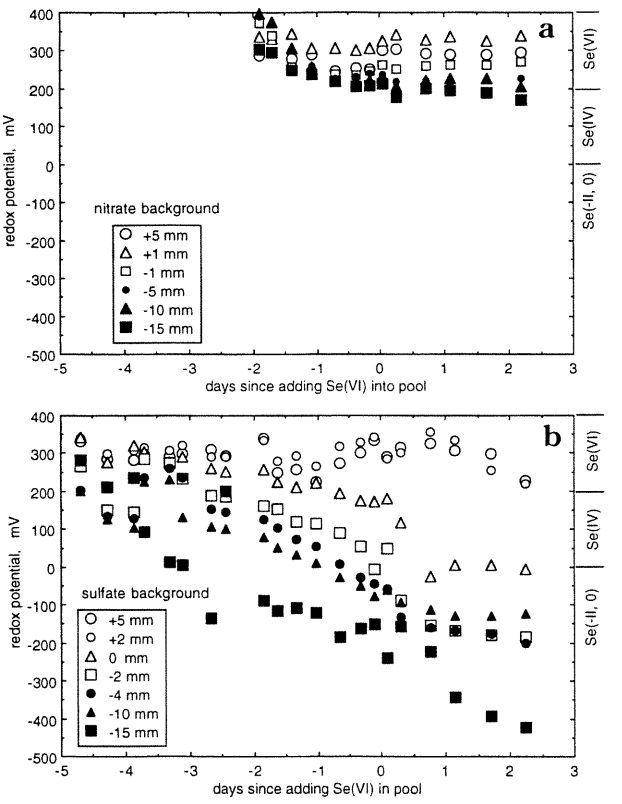


**FIGURE 2. Redox potential measurements in the pool–sediment system with nitrate (a) and without nitrate (b).**

micro-XANES of selected locations within columns. The ponding experiments ran for total elapsed times of about 62 h.

Micro-XANES spectra of selected locations within columns provided local Se speciation. Interpretation of oxidation state distributions within specific locations in the ponded sediment systems were based on comparing their micro-XANES with that of model Se compounds. Model compounds consisting of $Na_2SeO_4$ for Se(VI), $Na_2SeO_3$ for Se(IV), red Se(0), selenomethionine, and seleno-cystine were prepared by mixing into dry soil (the <52 $\mu$m fraction of Turlock sandy loam). The Se concentration in these solid standard samples ranged from 0.01 to 2 in mass percent. Aqueous standard samples of $Na_2SeO_4$ and $Na_2SeO_3$ solutions were also prepared at concentrations equal to 4.8 mM (380 mg of Se $L^{-1}$). For micro-XANES scans, the monochromatic X-ray energies ranged from −35 to +121 eV relative to the Se(0) K-edge. The subregion ranging from −15 to +30 (relative) eV was scanned in 0.35 eV steps, and the remaining regions were scanned in 3.5 eV increments. An efficient approach for obtaining micro-XANES maps of unknown systems relies on spatially scanning samples with the monochromator set sequentially to several characteristic energies that best distinguish the XANES of possible species (*37*). This approach was not taken here in an effort to better distinguish Se(0) from organo-Se forms that have relatively similar absorption edge energies. Instead, full micro-XANES spectra were collected at selected locations within samples. Micro-XANES spectra in the ponded sediment systems took 12 min to collect. Unlike stable model compounds, the micro-XANES collected in the ponded sediment systems were expected to be generally time-dependent. Thus, fast collection of spectra was preferred in order to obtain effectively instantaneous local Se speciation. Longer micro-XANES collection times could yield apparently higher quality spectra at the risk of including temporal

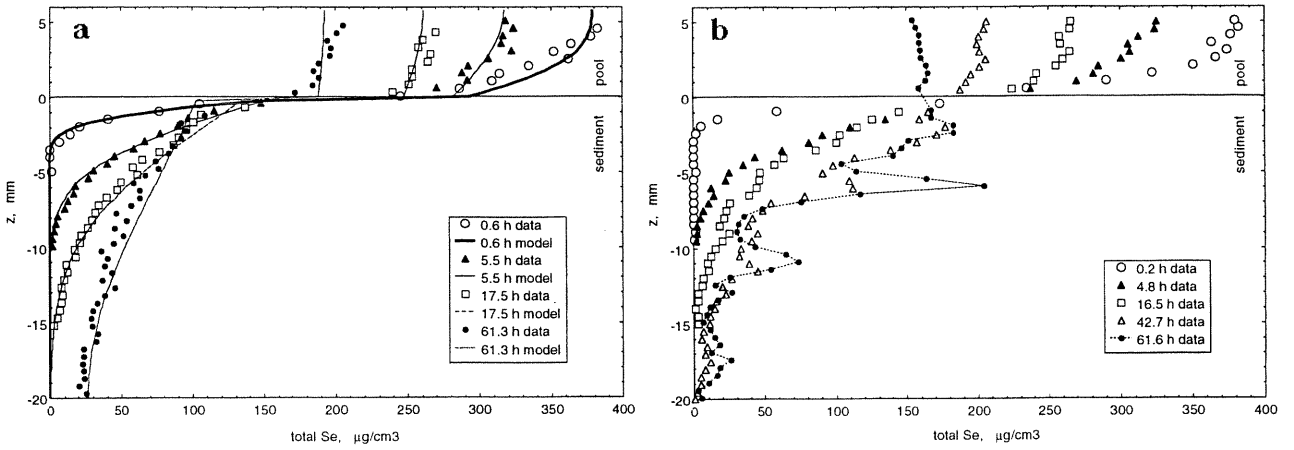


**FIGURE 3. Total Se profiles within pool–sediment columns at various times in the systems (a) with nitrate and (b) without nitrate. The SXRFM data are shown as points. Curves are results of finite difference modeling.**

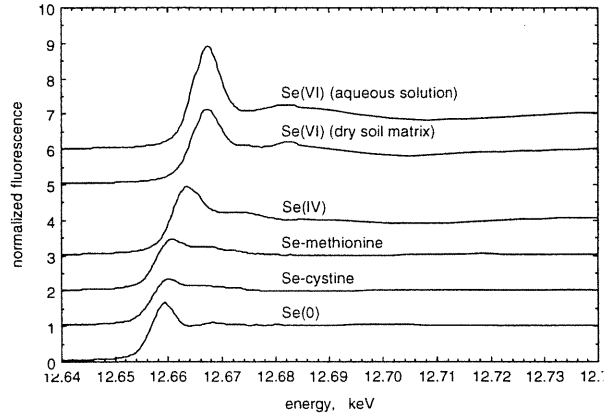


**FIGURE 4. Model Se XANES spectra used for interpreting micro-XANES measurements in ponded sediments.**

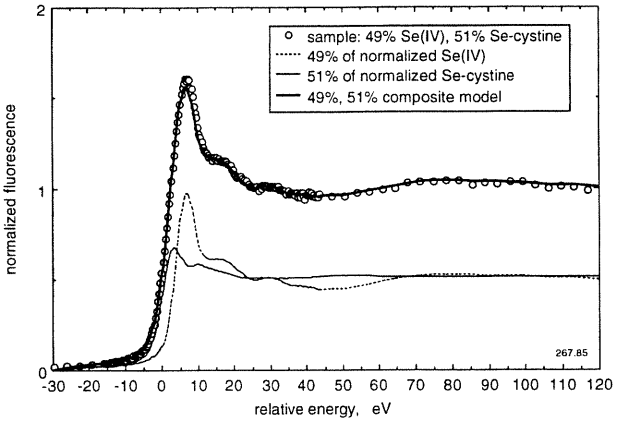


**FIGURE 5. Linear combination XANES fitting for known mixtures of Se standards [selenium cystine and Se(IV)] in the soil matrix.**

changes in speciation and concentration. The local micro-XANES spectra were later compared with various linear combination fits of model Se compounds in order to determine speciation.

## Results and Discussion

Redox potential measurements showed that oxidizing conditions were maintained throughout the experiment in both the ponded water and sediment of the +N system (Figure 2a). Most of these redox potentials in the +N system remained within the range of Se(VI) stability (*9*), although speciation and redox measurements are not expected to be quantitatively correlated (*39*). In contrast, gradients in redox potential quickly developed in the −N system, maintaining high values in the pool and progressively lower values in the sediment (Figure 2b). Pool water pH values were neutral (6.8−7.5).

Total Se concentration profiles from the two systems showed removal of Se from ponded waters and accumulation within shallow sediment (Figure 3a,b). Concentrations of total Se within waters and sediments were determined through calibration of normalized Se Kα fluorescence with the previously described standard (aqueous and sediment matrix) samples. The position of the pool–sediment boundary was located using the optical microscope of the SXRFM and coincided with the inflection region for the Fe and Zn fluorescence profiles. Measurements within about 0.5 mm of the sediment–water interface included influences from both the pool and sediment because of a combination of selected beam-size and sediment boundary roughness and therefore could not be quantitatively interpreted. Total Se concentrations obtained with the SXRFM in the $NO_3^-$-rich (+N) system exhibited a series of profiles that indicate that Se(VI) diffused freely into the sediment from the pool, without significant reduction to adsorbed or precipitated species (data points in Figure 3a). Micro-XANES analyses at various locations in the +N system showed that Se remained in the Se(VI) state throughout this experiment. All Se concentrations in Figure 3 are expressed on a mass per unit bulk volume basis in order to permit easier comparisons in these two-compartment systems. It should be noted that the times indicated for the experimental results in these figures are all ±0.08 h due to the 0.16 h scan times. The measurements of Se depth profiles in the +N system compare well with explicit finite difference model predictions based solely on diffusion, shown as curves in Figure 3a. The calculated profiles were obtained using measured diffusivities in water ($D_w = 3.6$ mm$^2$ h$^{-1}$), a fitted effective diffusivity in sediments ($D_s = 0.65$ mm$^2$ h$^{-1}$), and a harmonic mean diffusivity at the water–sediment interface (*33*). The effective diffusivity of Se(VI) in sediments was obtained by simultaneously fitting to all of the +N depth profiles. Its value is about half that estimated in the previous work (*33*), suggesting that reversible Se(VI) sorption–desorption is influencing transport (*40*).

The overall evolution of the total Se distribution within the sediments without $NO_3^-$ (Figure 3b) provided indirect evidence that reactions strongly influenced mass transfer. The rates of pool–sediment transfer of Se were more rapid into the $NO_3^-$-free organic matter-amended sediment, especially at later times. Reduction of Se(VI) within shallow sediments leads to increases in its concentration gradient at

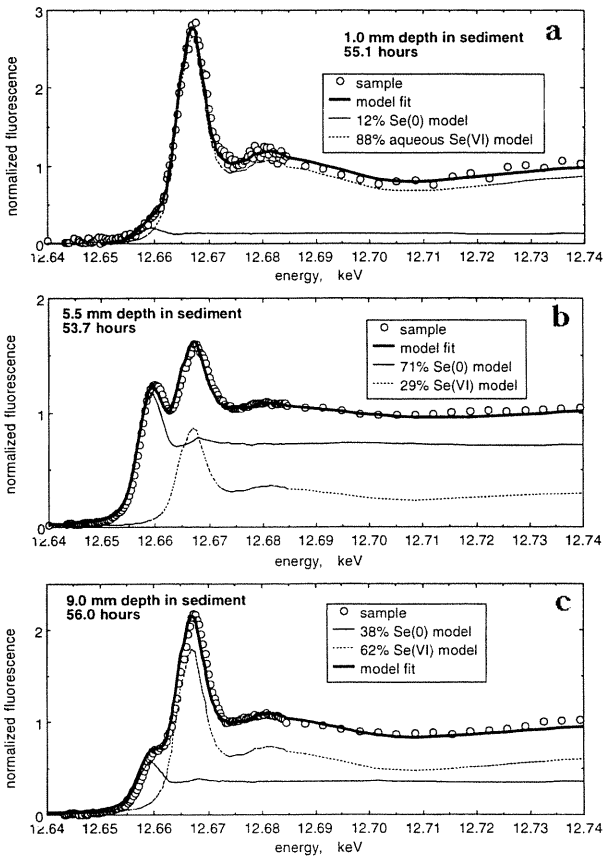


**FIGURE 6. Micro-XANES spectra from selected depths within the −N column: (a) 1.0, (b) 5.5, and (c) 9.0 mm depths.**

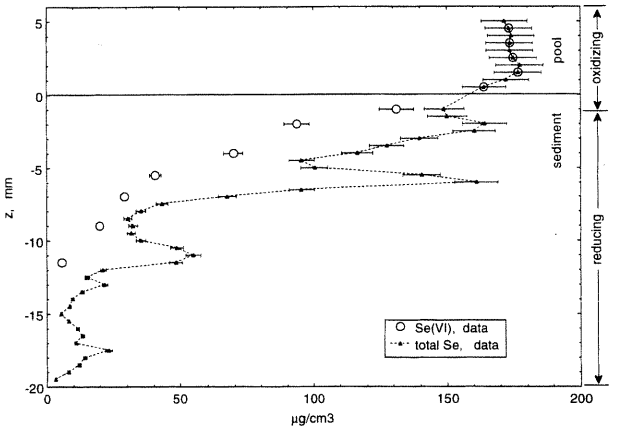


**FIGURE 7. Profiles of total Se and of Se(VI) in the −N sediment column at 56 ± 2 h.**

the pool−sediment boundary, thereby enhancing diffusive Se removal from pool waters. Note that local Se concentration maxima grow within the −N sediment profiles, indicating diffusion of soluble species to local regions of active Se sorption and/or precipitation. These observations demonstrate the need to augment total Se concentration profiles with micro-XANES information on Se valence speciation.

Micro-XANES spectra performed at key locations within these two systems provided insights into Se speciation. For this purpose, spectra were fit to linear combinations of XANES of model compounds (Figure 4). An example of linear combination fitting for a known mixture of Se standards [selenium cystine and Se(IV)] in the soil matrix is shown in Figure 5. Results from these and other linear combinations fitting to standard sample mixtures indicated that uncertainties were ±5% when unknown samples are comprised of mixtures of the tested model compounds. Similar uncertainties were assigned to Se XANES fits reported in previous studies (*31, 32*). Spectra collected within the ponded waters were best matched by that of the aqueous Se(VI) model, indicating that Se reduction within the surface water was not significant. Selected micro-XANES spectra collected at various depths within the −N sediment near the end of this ponding experiment are shown in Figure 6a−c, along with their best linear combination fits to model spectra. As shown in this figure, best fits were generally obtained using combinations of Se(0) and aqueous Se(VI) models. In a few of the cases in which Se(VI) was the dominant species, replacement of the Se(0) model with the selenium cystine model provided equally good fits. In all spectra with >50% of the Se in reduced form, use of the Se(0) model provided better matches than either of the organo-Se models (selenium cystine and selenium methionine). It is interesting to note that accumulation of the intermediate oxidation state, Se(IV), was typically less than 5% of the total local concentration (i.e., less than the uncertainty of our measurements).

The approximate profile of Se(VI) near the end of this experiment was reconstructed from fitted micro-XANES spectra collected at various depths. This result shows that enveloped within the irregular concentration profile of total Se is a monotonically decreasing Se(VI) profile, consistent with Se(VI) diffusion through a region with spatially varying Se(VI) reduction rates (Figure 7). Comparison of the total Se and Se(VI) profiles further shows that Se reduction within the upper 1 mm of sediment is relatively insignificant, a result consistent with an oxygen diffusion rate sufficient to sustain a thin layer of surface sediment under oxic conditions. The average behavior of this system with respect to pool Se removal can be modeled with an overall apparent first-order Se(VI) reduction rate constant, $k_r$, of 0.015 $h^{-1}$ applied to the deeper than 1 mm sediments in the diffusion simulations. This rate constant is within the range of values reported in a kinetic study (*41*). However, use of a uniform reduction rate constant results in development of only one maxima in the total Se profile (at the top of the assumed reducing zone). Recall that the micro-XANES information from the −N sediment column showed the development of several local maxima, indicating the existence of several local zones with significantly higher than average reduction rates. The micro-XANES results summarized in Figure 7 show that local rates of reduction to Se(0) varied in a heterogeneous manner and that reduction rates were up to 10 times greater in the more rapidly reducing zones, which were separated by distances of about 5 mm. The growth of such heterogeneity in total Se concentrations is interesting in that it evolved in the absence of a priori identifiable microsites for Se(0) precipitation. This is in contrast to our earlier experiments in which we showed Se(0) precipitation within and immediately around decomposing plant roots (*37, 42*). Despite the development of heterogeneously distributed reduction rates, a characteristic reduction zone thickness, $L_r$, can be determined through dimensional analysis (*43*):

$$L_r = \sqrt{\frac{D_s}{k_r}} \qquad (1)$$

Using the previously mentioned values of $k_r$ and $D_s$, an $L_r$ of 7 mm is obtained in the diffusion−reduction case, a result which is in the range revealed in the −N experiment. It should be noted that the Se(VI) concentrations initially ponded over the sediments in this study were $10^3$ times higher than those of drainwaters discharged into Kesterson Reservoir in order to permit rapid collection of micro-XANES spectra. The toxic effects of such high Se(VI) concentrations may have diminished microbial activity, resulting in a lower Se reduc-

tion rate. Studies of reduction in sediments at much lower Se(VI) concentrations (using the $^{75}Se$ radioisotope) have reported rate constants as high as 2.2 $h^{-1}$ (*44, 45*).

These results directly show that reduction of Se(VI) to Se(0) can occur within very shallow depths in reducing sediments. The necessary environmental condition for generation of such heterogeneity is a sharp gradient in redox status provided in the water–sediment boundary region. In previous studies (*37, 42*), we demonstrated how redox conditions at decomposing plant roots can generate local accumulation of insoluble Se species. In such local environments where strong redox gradients prevail, measurements with appropriate spatial resolution are required in order to be meaningfully interpreted. Volume averaging across such heterogeneity prevents observation of small scale processes that can control transport and overall reaction progress. Results from the two columns demonstrated how the balance between rates of diffusion and reduction determines the evolution of total Se profiles in hydrostatic, ponded sediments. Slower reduction rates permit Se(VI) diffusion deeper into sediments, more effective dissipation of concentration gradients, and therefore slower depletion from ponded waters. More rapid reduction rates prevent deep advances of the diffusion front, accumulation of reduced species at shallow depths, sustained high concentration gradients, and more rapid depletion of Se(VI) from ponded waters. Model results that are consistent with measurements in Kesterson Reservoir sediment cores are obtained by combining our average apparent first-order Se(VI) reduction rate with appropriate advection and dispersion terms (*46*). The fact that most of the Se contamination was restricted to very shallow depths in the advection–reduction dominated field setting can be concisely ascertained through the advection–reduction Damkohler number (*43, 47*)

$$D_{a,r} = \frac{k_r L_r}{v_p} \qquad (2)$$

where $v_p$ is the average pore water velocity. Setting $D_{a,r}$ to unity (to estimate conditions under which reaction and transport have similar influences) and using our previous value of $k_r$ and a Kesterson Reservoir average $v_p$ of 9 mm $d^{-1}$ (*48*), we obtain a value for $L_r$ of 26 mm. Other influences such as low $k_r$, macropore flow, and periodic drying of ponds contribute to larger values of $L_r$. Nevertheless, these considerations show that Se(VI) transport into reducing sediments is limited to distances on the order of $(D_s/k_r)^{0.5}$ or $v_p/k_r$, which can be very short.

The manner in which diffusion and reduction rates regulate Se mass transfer across static pond–sediment interfaces and the use of micro-XANES in investigating reactive transport across sharp environmental boundaries were illustrated in this real time, in-situ study. The observation of localized zones of Se(VI) reduction to Se(0) at very shallow depths demonstrates the importance of obtaining in-situ, highly spatially resolved information in real time. Conventional laboratory and field sampling methods cannot provide the resolution required to characterize transient reactive transport in regions with steep redox gradients.

## Acknowledgments

Research was in part carried out at the NSLS, Brookhaven National Laboratory, which is supported by the U.S. Department of Energy, Division of Material Sciences and Division of Chemical Sciences. We thank the staff of NSLS for providing the synchrotron radiation. We thank Satish C. B. Myneni, Geraldine M. Lamble, and the anonymous reviewers for their helpful comments. T.K.T. acknowledges funding through the Director, Office of Energy Research, Office of Basic Energy Sciences, Geosciences Program of the Department of Energy, under Contract DE-AC03-76SF00098. S.R.S., G.S.-M., and S.B. acknowledge support form U.S. Department of Energy Contracts DE-FG02-92BR14244 and DE-AC02-76CH00016. P.N. acknowledges support from Financial Assistance Award Number DE-FC09-96SR18546 from the U.S. Department of Energy to the University of Georgia Research Foundation and by ERDA/WSRC subcontract AA46420T.

## Literature Cited

(1) Berner, R. A. *Early Diagenesis, A Theoretical Approach*; Princeton University Press: Princeton, NJ, 1980.
(2) Stumm, W.; Morgan, J. J. *Aquatic Chemistry*, 3rd ed.; John Wiley and Sons: New York, 1996.
(3) Santschi, P.; Hohener, P.; Benoit, G.; Bucholtz-ten-Brink, M. *Mar. Chem.* **1990**, *30*, 269–315.
(4) Rosenfeld, I.; Beath, O. A. *Selenium Geobotany, Biochemistry, Toxicity, and Nutrition*; Academic Press: New York, 1964.
(5) *Selenium in Agriculture and the Environment*; Jacobs, L. W., Ed.; SSSAJ Special Publication No. 23; American Society of Agronomy: Madison, WI, 1989.
(6) *Selenium in the Environment*; Frankenberger, W. T., Jr., Benson, S. M., Eds.; Marcel Dekker: New York, 1994.
(7) Weres, O., Jaouni, A.-R.; Tsao, L. *Appl. Geochem.* **1989**, *4*, 543–563.
(8) Oremland, R. S.; Hollibaugh, J. T.; Maest, A. S.; Presser, T. S.; Miller, L. G.; Culbertson, C. W. *Appl. Environ. Microbiol.* **1989**, *55*, 2333–2343.
(9) Masscheleyn, P. H.; Delaune, R. D.; Patrick, W. H., Jr. *Environ. Sci. Technol.* **1990**, *24*, 91–96.
(10) Zhang, Y.; Moore, J. N. *Environ. Sci. Technol.* **1996**, *30*, 2613–2619.
(11) Myneni, S. C. B.; Brown, G. E., Jr.; Tokunaga, T. K. Stanford Synchrotron Radiation Laboratory 1996 Activity Report; Stanford, CA, 1997.
(12) Presser, T. S.; Barnes, I. *Water Resour. Invest.* (*U.S. Geol. Surv.*) **1985**, *No. 84-4220*.
(13) Ohlendorf, H. M. In *Selenium in Agriculture and the Environment*; Jacobs, L. W., Ed.; Soil Science Society of America Special Publication 23; American Society of Agronomy: Madison, WI, 1989; pp 133–177.
(14) Weres, O.; Bowman, H. R.; Goldstein, A.; Smith, E. C.; Tsao, L. *Water Air Soil Pollut.* **1990**, *49*, 251–272.
(15) Sposito, G.; Yang, A.; Neal, R. H.; Mackzum, A. *Soil Sci. Soc. Am. J.* **1991**, *55*, 1597–1602.
(16) White, A. F.; Benson, S. M.; Yee, A., W.; Wollenberg, H. A., Jr.; Flexser, S. *Water Resour. Res.* **1991**, *27*, 1085–1098.
(17) Lundquist, T. J.; Green, F. B.; Tresan, R. B.; Newman, R. D., Oswald, W. J. In *Selenium in the Environment*; Frankenberger, W. T., Jr., Benson, S., Eds.; Marcel Dekker: New York, 1994; pp 251–278.
(18) Kheboian, C.; Bauer, C. F. *Anal. Chem.* **1987**, *59*, 1417–1423.
(19) Gruebel, K. A.; Davis, J. A.; Leckie, J. O. *Soil Sci. Soc. Am. J.* **1988**, *52*, 390–397.
(20) Beckett, P. H. T. *Adv. Soil Sci.* **1989**, *9*, 143–176.
(21) Revsbech, N. P.; Jorgensen, B. B. *Adv. Microb. Ecol.* **1987**, *9*, 293–352.
(22) Jones, K. W.; Gordon, B. M. *Anal. Chem.* **1989**, *61*, 341A–358A.
(23) Sutton, S. R.; Rivers, M. L.; Bajt, S.; Jones, K. W. *Nucl. Instrum. Methods* **1993**, *B75*, 553–558.
(24) Brown, G. E., Jr.; Calas, G.; Waychunas, G. A.; Petiau, J. *Rev. Mineral.* **1988**, *18*, 431–512.
(25) Koningsberger, D. C.; Prins, R. *X-ray Absorption: Principles, Applications, Techniques of EXAFS, SEXAFS and XANES*; John Wiley and Sons: New York, 1988.
(26) Brown, G. E., Jr.; Parks, G. A. *Rev. Geophys.* **1989**, *27*, 519–533.
(27) Schulze, D. G.; Bertsch, P. M. *Adv. Agron.* **1995**, *55*, 1–66.
(28) Waychunas, G. A.; Apted, M. J.; Brown, G. E., Jr. *Phys. Chem. Miner.* **1983**, *10*, 1–9.
(29) George, G. N.; Gorbaty, M. L. *J. Am. Chem. Soc.* **1989**, *111*, 3182–3186.
(30) Vairavamurthy, A.; Manowitz, B.; Zhou, W.; Jeon, Y. In *Environmental Geochemistry of Sulfur Oxidation*; Alpers, C. N., Blowes, D. W., Eds.; American Chemical Society Symposium Series 550; American Chemical Society: Washington, DC, 1994; pp 412–430.
(31) Pickering, I. J.; Brown, G. E., Jr.; Tokunaga, T. K. *Environ. Sci. Technol.* **1995**, *29*, 2456–2459.
(32) Tokunaga, T. K.; Pickering, I. J.; Brown, G. E., Jr. *Soil Sci. Soc. Am. J.* **1996**, *60*, 781–790.

(33) Tokunaga, T. K.; Brown, G. E., Jr.; Pickering, I. J.; Sutton, S. R.; Bajt, S. *Environ. Sci. Technol.* **1997**, *31*, 1419−1425.
(34) Sutton, S. R.; Jones, K. W.; Gordon, B.; Rivers, M. L.; Bajt, S.; Smith, J. V. *Geochim. Cosmochim. Acta* **1993**, *57*, 461−468.
(35) Bajt, S.; Clark, S. B.; Sutton, S. R.; Rivers, M. L.; Smith, J. V. *Anal. Chem.* **1993**, *65*, 1800−1804.
(36) Bertsch, P. M.; Hunter, D. B.; Sutton, S. R.; Bajt, S.; Rivers, M. L. *Environ. Sci. Tech.* **1994**, *28*, 980−984.
(37) Sutton, S. R.; Bajt, S.; Delaney, J.; Schulze, D.; Tokunaga, T. *Rev. Sci. Instrum.* **1995**, *66*, 1464−1467.
(38) Krause, M. O.; Oliver, J. H. *J. Phys. Chem. Ref. Data* **1979**, *8*, 329−338.
(39) Runnells, D. D.; Lindberg, R. D. *Geology* **1990**, *18*, 212−215.
(40) Kemper, W. D. In *Methods of Soil Analysis, Part 1—Physical and Mineralogical Methods*, 2nd ed.; Klute, A., Ed.; American Society of Agronomy: Madison, WI, 1986; pp 1007−1024.
(41) Jayaweera, G. R.; Biggar, J. W. *Soil Sci. Soc. Am. J.* **1996**, *60*, 1056−1063.
(42) Tokunaga, T. K.; Sutton, S. R.; Bajt, S. *Soil Sci.* **1994**, *158*, 421−434.
(43) Massey, B. S. *Measurements in Science and Engineering*; Halsted Press: New York, 1986.
(44) Oremland, R. S.; Steinberg, N. A.; Maest, A. S.; Miller, L. G.; Hollibaugh, J. T. *Environ. Sci. Technol.* **1990**, *24*, 1157−1164.
(45) Steinberg, N. A.; Oremland, R. S. *Appl. Environ. Microbiol.* **1990**, *56*, 3550−3557.
(46) Tokunaga, T. K.; Bajt, S., Sutton, S. R.; Nuessle, P. *Extended Abstracts of the Fourth International Conference on the Biogeochemistry of Trace Elements*, Berkeley, CA, June 23−26, 1997; U.S. Army Cold Regions Research and Engineering Laboratory: Hanover, NH, 1997; pp 339−340.
(47) Phillips, O. M. *Flow and Reactions in Permeable Rocks*; Cambridge Unviversity Press: Cambridge, 1991.
(48) Benson, S. M.; White, A. F.; Halfman S.; Flexser, S.; Alavi, M. *Water Resour. Res.* **1991**, *27*, 1071−1084.

*Received for review July 28, 1997. Revised manuscript received December 18, 1998. Accepted January 26, 1998.*

ES9706559